PCCP

PAPER

View Article Online
View Journal | View Issue

Cite this: *Phys. Chem. Chem. Phys.*, 2015, **17**, 10108

Effects of separation distance on the charge transfer interactions in quantum dot–dopamine assemblies†

Xin Ji, Wentao Wang and Hedi Mattoussi*

Received 24th January 2015,
Accepted 3rd March 2015

DOI: 10.1039/c5cp00462d

www.rsc.org/pccp

We explored the effects of changing the separation distance on the charge transfer interactions between luminescent QD and proximal dopamine (in QD–dopamine assemblies), and the ensuing photoluminescence (PL) quenching. The separation distance was controlled using a tunable size bridge between the QD and dopamine *via* a poly(ethylene glycol) (PEG) chain where the average number of monomers was discretely varied. Using steady-state and time-resolved fluorescence measurements, we found that the photoluminescence losses were substantially more pronounced for QD–dopamine complexes prepared with the shortest PEG bridge, but progressively decreased with increasing PEG size. We also found that the charge transfer interactions can be affected by the nature of the capping ligand used. In particular, we found that interactions and PL quenching in these assemblies tracked the effects of separation distance, conjugate valence and the energy mismatch between the dopamine redox levels and QD energy levels, when a compact zwitterion was used to control the conjugate configuration. However, additional effects of shielding the access of reactive dopamine to amine groups on the QD surface, when a longer inert PEG ligand was used, were found to produce heterogeneous conjugates, alter the interactions and produce weaker PL quenching.

Introduction

Semiconductor quantum dots (QDs) possess several unique electronic and optical properties with size- and composition-tunable excitation and emission spectra.[1–4] Colloidal CdSe–ZnS core–shell QDs, for example, exhibit a remarkable resistance to photo- and chemical degradation, and they have large absorption cross-section combined with narrow emission profiles that span the visible spectrum.[5–9] These nanocrystals have large surface-to-volume ratio with a large fraction of their atoms arrayed at the surfaces. They are stabilized with capping molecules, which can be modified, allowing one to disperse them in various solution media. These capping molecules provide electronic passivation of the surface. The photoemission properties of these materials can be highly sensitive to the nature of the surface ligand and/or to interactions with proximal dyes, redox complexes and certain metal ions.[10–15] As a result, they offer excellent platforms for developing sensors based on energy transfer and/or charge transfer interactions.[13–19] Moreover, these systems offer great flexibility as control over the number of dyes and/or complexes brought in close proximity to the QD surface can be achieved. Combined with the ability to tune the particle size, separation distance and spectral overlap, QD-conjugated to fluorescent dyes (or proteins) and redox-active complexes provide a rich and challenging system to investigate and understand.

Over the past decade, several studies focusing on the fabrication of hybrid QD-assemblies where control over separation distance and conjugate architecture have been reported.[18,20–22] In one example, Watson and co-workers probed the distance-dependent electron transfer between CdS QDs and TiO_2 nanoparticles coupled through the use of bifunctional mercaptoalkanoic acid bridges with varying alkyl chain lengths.[21] They attributed the measured changes in the QD spectroscopic properties to electron transfer from photoexcited CdS QDs to the linked TiO_2 nanoparticles.[21] They found that the electron transfer efficiency decreased dramatically with increasing alkyl chain length (due to increased interparticle separation). In another example, Zhao and co-workers explored the use of CdSe–ZnS QDs coupled to gold nanoparticles *via* a complementary oligonucleotide sequences to investigate the distance dependence of metal-enhanced QD fluorescence in QD–DNA–Au assemblies.[23] The assemblies were constructed by linking QDs to gold nanoparticles through complementary oligonucleotide sequences of varying size. They reported that ~2.5 enhancement in the QD emission for separation distance of ~12 nm.[23] In a third example, we probed the PL quenching of CdSe–ZnS QDs conjugated to fluorescent gold

Department of Chemistry and Biochemistry, Florida State University, 95 Chieftan Way, Tallahassee, Florida 32306, USA. E-mail: mattoussi@chem.fsu.edu

† Electronic supplementary information (ESI) available: Additional experimental details on the experimental set up, data analysis, QD growth, ligand synthesis, ligand exchange, coupling reaction and conjugate purification are provided. See DOI: 10.1039/c5cp00462d

nanoclusters in buffer media,[22] where we tested the effects of varying the spectral overlap and separation distance on the QD photoluminescence. In particular, we measured strong PL loss but no enhancement in the cluster emission.

Dopamine is a neurotransmitter that plays a significant role in the brain activity and behavior.[24–26] It transmits information from one neuron to the next through chemical signals, and is closely associated with reward-seeking behaviors (*e.g.*, addiction); drastic changes in dopamine levels are associated with dysfunctions of the nervous system (*e.g.*, low dopamine levels are measured for patient with Parkinson's disease).[27–29]

Interactions of dopamine and its derivatives with luminescent QDs have been explored by several groups, due to the complex redox interactions and potential relevance in biology.[30–33] QD–dopamine complexes also provide a great platform for investigating the charge transfer interactions where control over the energy mismatch between the QD conduction and valence bands and dopamine oxidation potentials, as well as the valence of the conjugate can be realized.[32,33] For instance, we have previously explored the effects of tuning the redox coupling in hybrid assemblies by varying the pH of the buffer and QD size on the nature of the redox interactions and the ensuing changes in the QD optical and spectroscopic properties.[32–34]

In this report, we investigate the effects of varying the separation distance on the efficiency of charge transfer (CT) interactions in QD–dopamine conjugates using steady-state and time-resolved fluorescence measurements. The separation distance is tuned *via* a poly(ethylene glycol) (PEG) bridge with varying chain length, namely PEG_{200}, PEG_{400}, PEG_{600} and PEG_{1000}. The PEG bridge (part of the surface capping ligand) is sandwiched between a dihydrolipoic acid anchoring group and a terminal amine used for attaching the redox active dopamine (see Fig. 1). The conjugate design is further combined with mixed ligand exchange to control the number of reactive groups per QD and the nature of the inert ligand used (a terminally-inert PEG_{750} *vs.* a compact zwitterion). We measured a PL

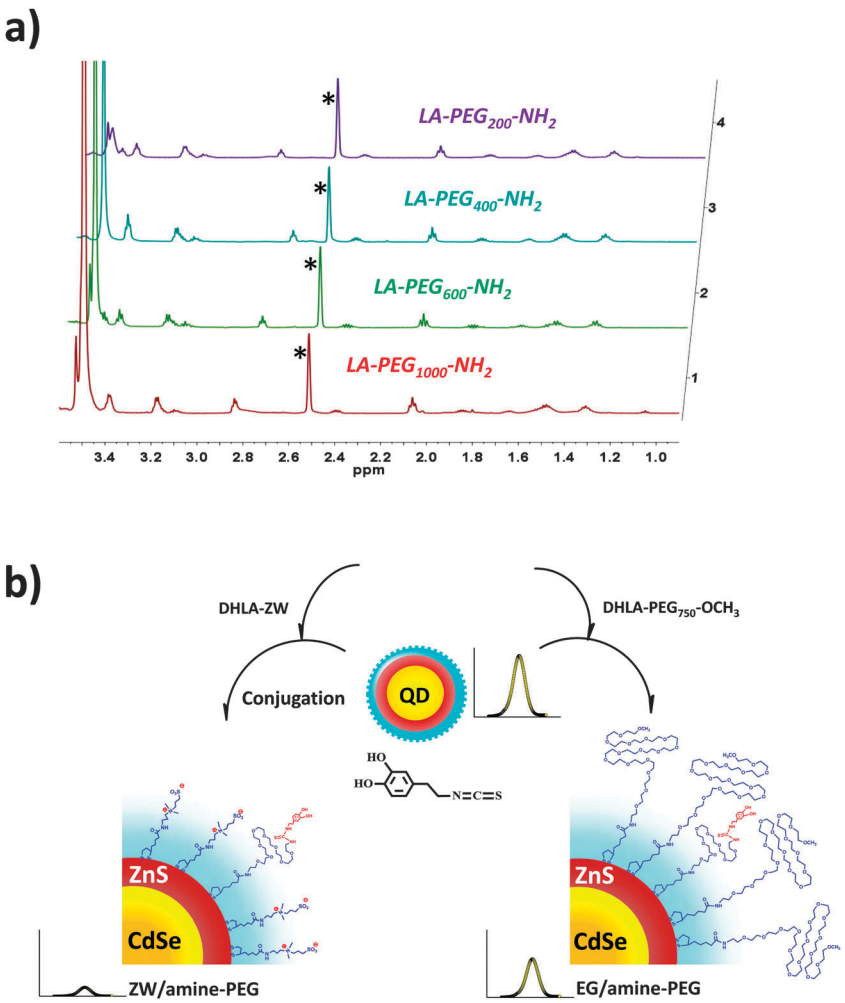

Fig. 1 (a) Stacked ^{1}H NMR spectra collected from LA-PEG-NH_2 ligands with variable PEG size. The pronounced peak at ~3.5 ppm is attributed to the protons in the PEG chain. The spectra were collected from ligands dissolved in DMSO. The sharp peak at ~2.5, denoted by *, is due DMSO in the medium. The plots show that the intensity of the proton peak from the PEG moiety increases with the average number of repeat PEG units per ligand. (b) Schematic representation of QD–dopamine conjugate assembly prepared using 5% DHLA-PEG_{400}-NH_2 mixed with either 95% DHLA-ZW, or DHLA-PEG_{750}-methoxy. The insets represent changes in the PL emission.

quenching efficiency that closely tracked the conjugate valence, but more importantly strongly depended on the size of the PEG bridge used. Moreover, we found that the nature of the inert ligands used in the mixed surface cap affects the rate of charge transfer and the resulting PL quenching. For instance, we found that when the inert ligand was switched from a zwitterion-modified dihydrolipoic acid (DHLA-ZW) to PEG_{750}-OMe-appended dihydrolipoic acid (DHLA-PEG_{750}-OMe) the larger PEG moieties shielded the access of dopamine to the amine groups on the QD surface, weakening the CT transfer interactions and producing lower PL quenching.

Results and discussions

Conjugate design and control of the QD-to-dopamine separation distance

Our conjugate design combines the use of mixed ligand exchange and lipoic acid appended with polyethylene glycol moieties as means to control the separation distance between the QD and dopamine as well as the number of dopamines per conjugate. It also provides a symmetric conjugate made of several redox groups positioned at the same distance from the QD center. We carried out ligand exchange on the QDs using a mixture of 95% inert ligands and 5% DHLA-PEG-amine ligands having varying PEG bridges, PEG_{200} (3 EG units), PEG_{400} (8 EG units), PEG_{600} (12 EG units), and PEG_{1000} (20 EG units). We also used two sets of inert ligands: DHLA-ZW (molecular scale) and DHLA-PEG_{750}-OMe (a short oligomer). The QDs capped with mixtures of 5% DHLA-PEG-NH_2 and 95% DHLA-PEG_{750}-OCH_3 will be referred to as EG/amine-PEG-QDs, while those prepared using a mixture of 5% DHLA-PEG-NH_2 and 95% DHLA-ZW will be referred to as ZW/amine-PEG-QDs. QDs prepared with 100% DHLA-PEG_{750}-OMe or 100% DHLA-ZW, referred to as neutral (*i.e.*, non-reactive), were used for control experiments. Following phase transfer to water media, the nanocrystals were covalently coupled to dopamine-isothiocyanate (dopamine-ITC), *via* amine-to-ITC reaction, using molar excess of dopamine-ITC.[33] In addition, by varying the nature and size of the inert ligand (which represents 95% of the total surface cap) from DHLA-ZW to DHLA-PEG_{750}-OMe we were able to investigate how the effects of shielding dopamine-ITC access to the amine groups on the QD surfaces can affect the PL quenching. Here, we anticipated that using DHLA-PEG_{750}-OMe as the inert ligand would shield access of the dopamine-ITC to the amine groups on the QD surface, thus reducing the redox coupling efficiency and the ensuing changes in the QD PL. In contrast, the more compact DHLA-ZW ligand would permit easier access of dopamine-ITC to the QD surface, resulting in stronger interactions and higher quenching (see Fig. 1). We should emphasize that coupling of the dopamine to the QDs is specifically driven by the reaction of ITC with the amine groups present on the PEG coating.[33] Physisorption and/or non-specific stickiness on the nanocrystal surfaces are negligible, given the nature of the polyethylene glycol capping shell used, and as verified using control dispersions made of 100% methoxy-PEG-capped QDs.[33,34]

Steady-state and time-resolved fluorescence measurements

1. QD–dopamine conjugates prepared with ZW/amine-PEG-QDs. Fig. 2a–d shows representative PL spectra collected from several dispersions of red-emitting QD–dopamine conjugates prepared using various PEG bridges: ZW/amine-PEG_{1000}-QDs (2a), ZW/amine-PEG_{600}-QDs (2b), ZW/amine-PEG_{400}-QDs (2c) and ZW/amine-PEG_{200}-QDs (2d). The data show that a progressive PL loss is measured when the dopamine-ITC molar concentration is increased for all sets of QD–dopamine assemblies studied, an observation that is fully consistent with previous findings on QD–dye and QD–redox-complex assemblies.[20,30,33,35] For the same set of QDs, the PL losses were largest for the shortest PEG bridge (PEG_{200}) and deceased with increasing PEG size to reach their lowest values measured for the PEG_{1000}. Furthermore, substantially larger PL losses were measured for the conjugates prepared using yellow-emitting QDs compared to their red-emitting counterparts (see Fig. 2e and f). The PL quenching efficiency, E, data shown in Fig. 2e and f were extracted from the steady-state fluorescence data, using the expression, $E = 1 - F_{DA}/F_D$, where F_{DA} and F_D designate the PL intensity measured for dispersions of QD–dopamine conjugates and QDs alone (control, without dopamine complexes), respectively. Images from selected dispersions of these conjugates under UV illumination, shown in Fig. 2g and h, provide a visual confirmation of the effects of varying the separation distance (and valence) on the degree of PL losses. In particular, dispersions of yellow-emitting QDs prepared with PEG_{200} bridge exhibit a near total quenching of the emission at all dopamine-to-QD ratios used.

The data on the quenching efficiency shown in Fig. 2e and f indicate that the overall trend can be fit using an expression of the form:[33]

$$E = \frac{\alpha' C_{dop}}{\alpha' C_{dop} + K'} \quad (1)$$

where α' and K' are parameters that depend on the relative alignment of the redox levels of the dopamine with respect to the energy levels of the QD and the separation distance, respectively. Such expression is consistent with a configuration where each conjugate is made of a central QD surrounded by several dopamines positioned at a fixed average separation distance, r, from the QD center (*i.e.*, centro-symmetric conjugate, see Fig. 1). The above behavior is consistent with the predicted expression for the dependence of E *vs.* valence, n, given by:[13,33]

$$E = \frac{\alpha n}{\alpha n + K} \quad (2)$$

Here α, K are directly related (proportional) to α' and K', respectively.[33] The conversion from eqn (1) (for E *vs.* C_{dop}) to eqn (2) (for E *vs.* n) is permitted by the fact that the number of coupled dopamines per QD in the final assemblies is expected to be proportional to the concentration of dopamine-ITC used in the reaction; amine-to-ITC coupling obeys the first-order bimolecular reaction.[36] We should also note that heterogeneity in the conjugate valence is an intrinsic property of QD-conjugates, and ideally should be taken into account when analyzing the dependence of the quenching efficiency on the dopamine-to-QD ratio

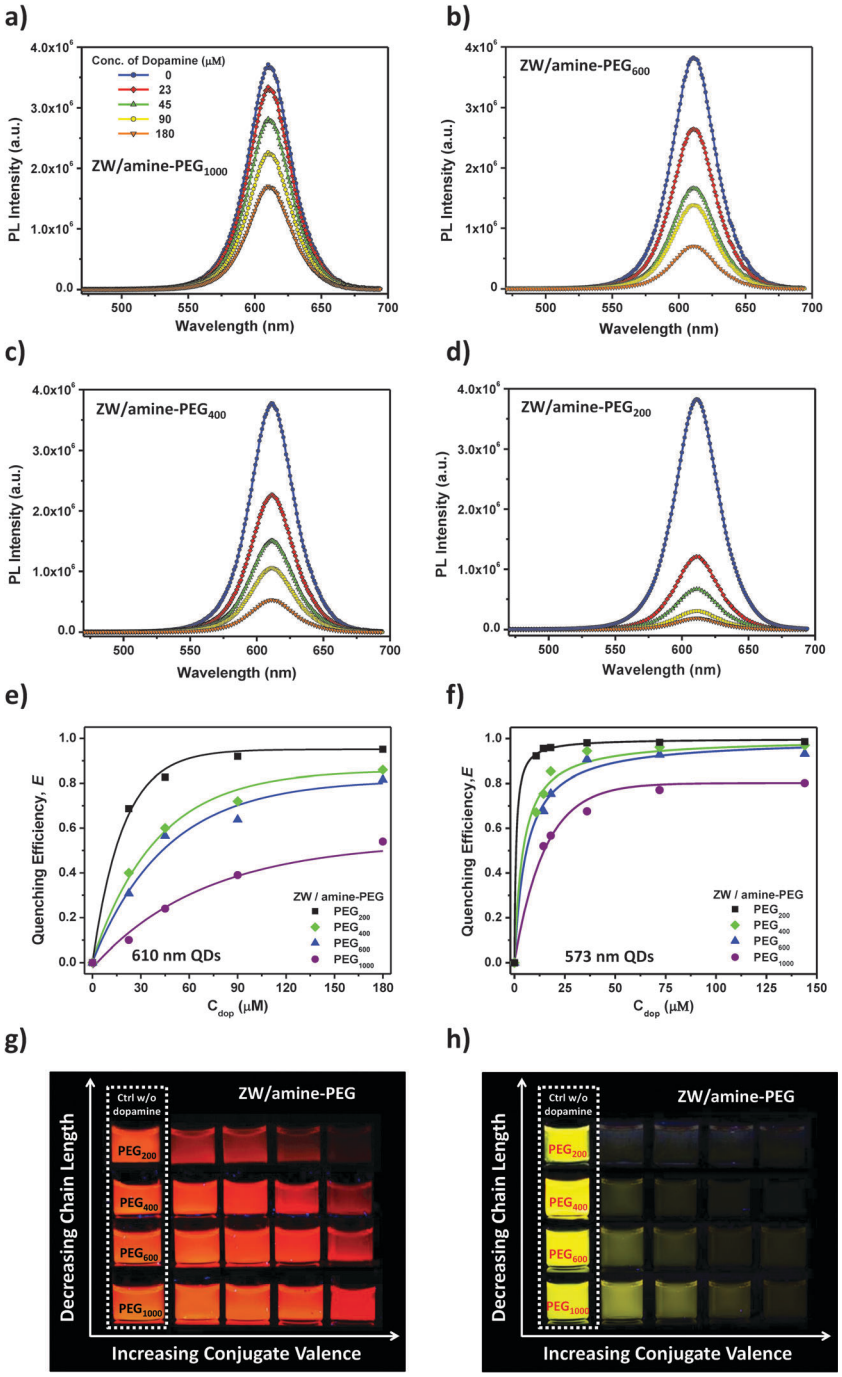

Fig. 2 (a–d) PL spectra collected from ZW/amine-PEG-QD-dopamine conjugates dispersed in DI water (at pH ~6.5) for increasing molar concentrations of dopamine-ITC and varying bridge size: (a) PEG_{1000}, (b) PEG_{600}, (c) PEG_{400} and (d) PEG_{200}; red-emitting QDs were used. (e) Cumulative plots of the quenching efficiency, *E*, *versus* C_{dop} for the above four sets of red-emitting ZW/amine-PEG-QDs. (f) Cumulative plots for *E versus* C_{dop} for conjugates prepared with the yellow-emitting ZW/amine-PEG-QDs. (g and h) Fluorescence images of selected dispersions of red- and yellow-emitting QD–dopamine conjugates under UV illumination.

(valence, *n*). In such case accounting for the heterogeneity is achieved using the Poisson statistics and fitting the quenching data using an equation of the form:[37]

$$E(N) = \sum_{n=1}^{N} p(N,n)E(n) \text{ with } p(N,n) = N^n \frac{e^{-N}}{n!}, \qquad (3)$$

where *N* is the average dopamine-to-QD ratio used and *n* is the exact number of dopamine groups attached to a single QD. The Poisson distribution function, $p(N,n)$, accounts for heterogeneity in the conjugate valence, and $E(n)$ is given by eqn (2) above.[37] We have found that fitting the quenching data using eqn (3) (after converting the concentration dependence to

valence dependence) provides minimal improvement in the data fit for the set of conjugates prepared using ZW/amine-PEG-QDs. Thus, fitting the data compiled in Fig. 2e and f using eqn (1) yielded values for K'/α' that depend on the bridge size and the QD size (band gap), with K'/α' = 69.4 (PEG_{1000}), 43.4 (PEG_{600}), 32.3 (PEG_{400}) and 9.7 (PEG_{200}) for red-emitting ZW/amine-PEG-QD-dopamine conjugates; similarly we extracted values that are consistently smaller for the set of yellow-emitting ZW/amine-PEG-QD-conjugates: K'/α' = 20.7, 10.8, 9.0 and 3.8, respectively. These findings clearly indicate that the quenching efficiencies are larger for smaller size QDs (those with wider band gap), due to a larger energy mismatch with the redox levels of dopamine.

The above steady-state data were further supported and complemented by time-resolved fluorescence measurements, where faster PL decays (indicative of a shortening in the QD PL lifetime) were observed for dispersions of QD-assemblies with increasing valences compared to the control sample (C_{dop} = 0) (see Fig. 3 and Fig. S3, ESI†). Moreover, shorter lifetimes were measured for the smaller size QDs and shorter PEG bridges. The above time-resolved PL data can be used to extract estimates for the charge-transfer rate constant (k_{CT}), defined as:[18,38,39]

$$k_{CT} = \frac{1}{\tau_{DA}} - \frac{1}{\tau_{D}} \quad (4)$$

Table 1 summarizes the experimental values for the yellow and red-emitting QD-dopamine conjugates prepared with various size PEG bridges and with a nominal dopamine-ITC : amine ratio of 7.5 : 1. There is a pronounced increase in k_{CT} from 5.92 × 10^7 s^{-1} for PEG_{1000} to 5.43 × 10^8 s^{-1} for PEG_{200} (*i.e.*, nearly a 10-fold increase) measured for yellow-emitting QD–dopamine conjugates prepared using ZW/amine-PEG-QDs. In comparison, a less pronounced increase in the transfer rate constant was measured for conjugates prepared with the red-emitting QDs. This confirms that the charge transfer interactions are also strongly affected by the QD size, in addition to the separation distance. The yellow-emitting (smaller radius) QDs have a larger band gap and provide more favorable mismatch in the energy levels between QDs and dopamines, promoting more efficient charge transfer interactions.

2. QD–dopamine conjugates prepared with EG/amine-PEG-QDs. Fig. 4a shows plots of the PL quenching efficiencies (E *vs.* C_{dop}) at the various PEG bridges for conjugates prepared using PEG_{750}-methoxy as the inert ligand in the mixed surface design, together with fits using eqn (1); yellow-emitting QD-conjugates are shown. The data show that there is a reasonable agreement between the PL quenching efficiencies measured for the present set and those shown in Fig. 2f above for the larger size bridges (PEG_{1000}, PEG_{600} and PEG_{400}), even though, the values measured for the EG/amine-PEG-QDs are consistently smaller than those measured for ZW/amine-PEG-QDs shown in

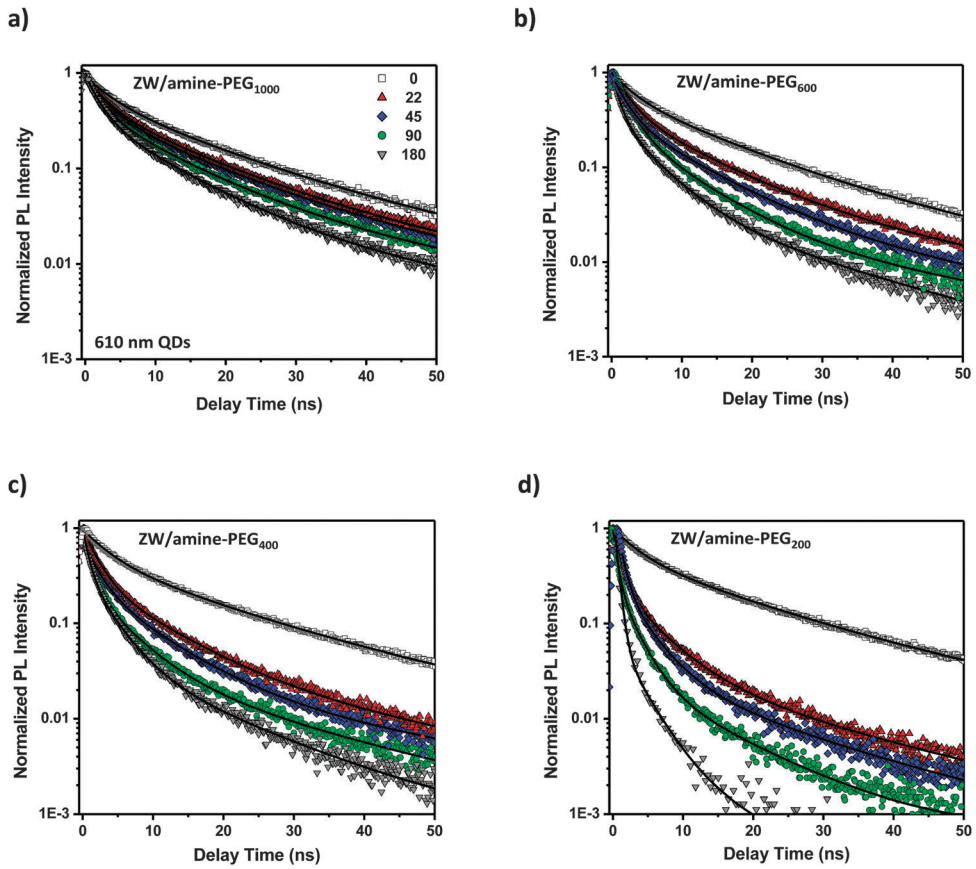

Fig. 3 Normalized time-resolved PL decay profiles for the conjugates prepared using red-emitting ZW/amine-PEG-QDs with increasing concentration of dopamine-ITC (top to bottom: 0, 22, 45, 90, 180 μM) for (a) PEG_{1000}, (b) PEG_{600}, (c) PEG_{400} and (d) PEG_{200}.

Table 1 Experimental values for the charge-transfer rate constant (k_{CT}) for all four sets of yellow and red-emitting QD–dopamine conjugates prepared using ZW/amine-PEG-QDs extracted from the TR fluorescence data. The conjugates were prepared with a nominal dopamine-ITC : amine ratio of 7.5 : 1 in DI water

	Yellow QDs; $\lambda_{em/max}$ = 573 nm			Red QDs; $\lambda_{em/max}$ = 610 nm		
Bridges	τ_D (ns)	τ_{DA} (ns)	k_{CT} (s^{-1})	τ_D (ns)	τ_{DA} (ns)	k_{CT} (s^{-1})
DHLA-PEG_{1000}-NH_2	20.01	9.16	5.92×10^7	19.78	16.07	1.17×10^7
DHLA-PEG_{600}-NH_2	20.20	4.81	1.58×10^8	20.44	13.00	2.80×10^7
DHLA-PEG_{400}-NH_2	21.00	3.46	2.41×10^8	22.45	11.38	4.33×10^7
DHLA-PEG_{200}-NH_2	20.38	1.69	5.43×10^8	22.65	8.18	7.81×10^7

Fig. 2f. However, the data collected from dispersions of conjugates prepared with the shortest PEG bridge (PEG_{200}) exhibit a rather unusual behavior with smaller measured quenching efficiencies that level off at higher C_{dop}. We also found that fitting the corresponding PL quenching data using eqn (1) does not provide a good agreement with the data for PEG_{200} (see dashed line in Fig. 4a). We attribute this difference to the effects of shielding the dopamine-ITC access to the amine groups on QD surface when a full size PEG_{750} is used as the inert ligands, which may produce smaller number of dopamine per conjugate and more heterogeneous valence. Such screening affects all sets of the QD–dopamine conjugates regardless of the bridge size. However, they would be more pronounced for the smaller PEG bridges, in particular for PEG_{200}. We take into account the effects of heterogeneity in the conjugate valence for EG/amine-PEG_{200}-QDs conjugates using Poisson correction (eqn (3)). Clearly, such correction provides a better fit for the quenching efficiency data as shown in Fig. 4b (solid black line). No sensible improvement could be measured when fitting the other data shown in Fig. 4b. Additional data on the steady-state and time-resolved fluorescence spectra of EG/amine-PEG-QD-conjugates dispersions are provided in the ESI† (Fig. S4 and S5).

Discussion and mechanism for the QD emission quenching

There are three major findings that can be highlighted from our measurements: (1) The PL quenching efficiency strongly depends on the PEG bridge size (*i.e.*, separation distance) between QDs and proximal dopamine, with higher efficiencies measured for QD–dopamine conjugates assembled with a shorter PEG moiety, and *vice versa*. In addition, for a given PEG size the efficiency tracks the conjugate valence. (2) We measured larger quenching efficiencies for the yellow-emitting QDs (smaller size) compared with their red-emitting (larger size) counterparts when the same size bridge was used. (3) The QD PL losses also depend on the type of mixed ligands used. By changing the size and the nature of the inert ligand, we were able to explore the effects of ligands shielding on the dopamine-ITC-to-amine coupling reaction and measured quenching efficiency. For instance, using mixed surface QDs prepared with 95% zwitterion promoted better access of the dopamine-ITC to the amine groups compared to the case where larger PEG_{750}-methoxy were used.

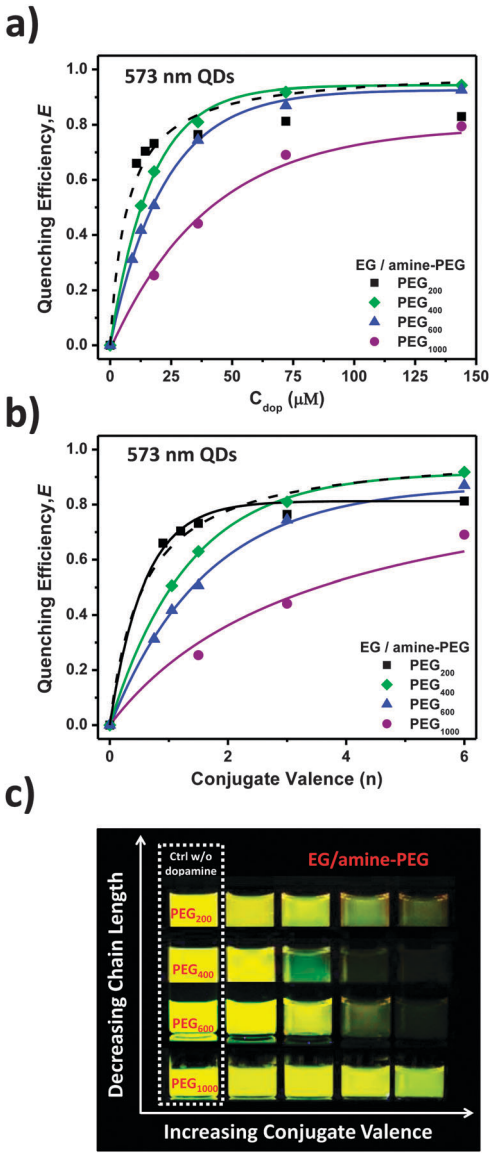

Fig. 4 (a) Plots of the quenching efficiencies (E *vs.* C_{dop}) for the various PEG bridges collected from QD–dopamine conjugates prepared using yellow-emitting EG/amine-PEG-QDs along with fits using eqn (1) but without accounting for the conjugate heterogeneity. (b) Plots of E *vs.* valence n together with fits using eqn (2), for $PEG_{400/600/1000}$ and fit to eqn (3) (accounting for the Poisson correction, dashed line) for PEG_{200}. (c) Images of selected dispersions of yellow-emitting QD–dopamine conjugates prepared using EG/amine-PEG-QDs under UV illumination.

We now discuss the above findings within the framework of charge transfer interactions between dopamine and photoexcited QDs. We have previously shown that in these assemblies a photoexcited QD interacts with two distinct species (the reduced catechol and the oxidized quinone) that coexist within the same conjugate, with: (1) electron transfer from the catechol to the valence band of the QD; and (2) electron transfer from conduction band of the QD to the oxidized quinone. These CT pathways are strongly affected by the medium pH, and combined they alter the electron–hole recombination, resulting in PL quenching of the QD.[33,34] Here, we analyze

the effects of varying the separation distance on the charge transfer interaction, by maintaining a fixed pH (at ~pH 6.5) and valence. At this pH we estimate, based on the Henderson–Hasselbalch relation (pH = pK_a − $\log_{10}$[catechol/quinone]) that the catechol-to-quinone molar ratio in the dispersion is ~1000-to-1; we used pK_a = 9.3 for this estimate.[40] This implies that within the present conditions, pathway 1 (see Fig. 5a) plays a dominant role in the charge transfer interactions in QD–dopamine conjugates. We thus limit our analysis to interactions involving electron transfer (ET) from the catechol groups to the valence band of a photoexcited QD (*i.e.*, $k_{CT} \equiv k_{ET}$, see Fig. 5a). We would like to stress that potential contribution of defects in the ZnS shell to the CT interactions between the dopamine and QDs are not at the origin of the differences in PL changes measured for the two sets of QDs. The overall thickness of the ZnS shell is similar for both sets and the separation distances used account for all relevant contributions (core–shell radius and ligand structure, see below). The measured differences are mainly due to changes in the energy mismatch between the QDs and proximal redox complex as discussed in our recent report.[34]

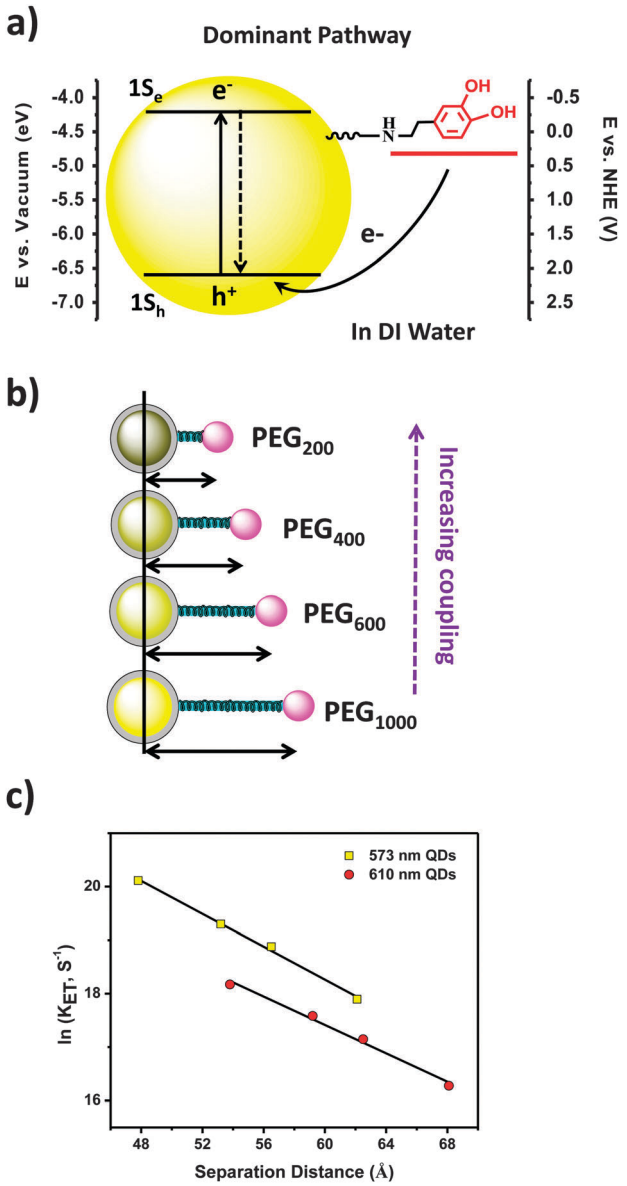

Fig. 5 (a) Schematic representation of the dominant charge transfer interaction pathway between QDs and proximal dopamine in DI water. The redox levels of dopamine at pH 6.5 were extracted from cyclic voltammograms (reported in ref. 33) for dispersions of dopamine-PEG-methoxy in buffer media. (b) Schematic representation of the anticipated changes in the separation distance and the corresponding electronic coupling strength (H) on the charge transfer interactions. (c) The dependence of electron transfer rate constant *versus* center-to-center separation distance for yellow- and red-emitting QD–dopamine conjugates prepared using ZW/amine-PEG-QDs. Lines are fit to the data using eqn (8).

To exploit the data on the quenching efficiency and extract a correlation between ET interactions and the separation distance, we first develop an estimate for the PEG size using the concept of excluded volume interactions developed by Flory for flexible polymers in good solvent conditions.[41] Indeed, polyethylene glycol is a flexible polymer highly compatible with water. In good solvent conditions, a polymer chain exhibit a coil like conformation, due to a balance between the excluded-volume interactions, which tend to expand its random configuration, and elastic restoring forces, which reduce its 3-dimensional expansion (swelling). The resulting end-to-end distance, R_f, for the PEG chain can be given by:[42–44]

$$R_f = a(M)^{\frac{3}{5}} \quad (5)$$

Here, a and M respectively designate the monomer size (3.5 Å for an ethylene glycol), and the number of repeat units per chain. The corresponding size for the various PEG bridges used, along with corresponding center-to-center separation distance, r, anticipated for the yellow and red-emitting QD–dopamine conjugates are compiled in Table 2.

We now correlate the experimental charge transfer rates extracted from the fluorescence data shown in Table 1 to the theoretical model of electron-transfer between two states developed by Marcus in 1956.[45] This theory has been successfully used to describe photoinduced electron transfer processes for an array of systems, and more recently to describe the electron transfer interactions between semiconductor QDs (as donor) and metal oxide nanoparticles and/or redox molecules (as acceptors) by Kamat and co-workers and Lian and co-workers.[46–48]

Within this description, the electron transfer rate from a single donor state (here a catechol) to a continuum of acceptor states (such as the valence band of the QD) can be expressed as:[47]

$$k_{ET} = \frac{2\pi}{h}\frac{H^2}{\sqrt{4\pi\lambda k_B T}} e^{\left\{-\frac{(\Delta G+\lambda^2)}{4\lambda k_B T}\right\}} \quad (6)$$

where k_B is Boltzmann constant, h is Planck's constant, and e is the elementary charge. ΔG is the change in the free energy of the system (associated with energy level mismatch between the donor and acceptor and is independent of the bridge size), λ is the system reorganization energy and H is the electronic coupling strength between donor and acceptor states. This parameter H accounts for the dependence of k_{ET} on the separation distance.

Table 2 Size for PEG bridges along with center-to-center separation distance extracted from conformation consideration detailed in the text

	Ligands	Repeat unit	R_f (Å)	Center-to-center distance,[a] r (Å)	
				Yellow-emitting QDs	Red-emitting QDs
Reactive ligands	DHLA-PEG$_{200}$-NH$_2$	3	6.8	47.8	53.8
	DHLA-PEG$_{400}$-NH$_2$	8	12.2	53.2	59.2
	DHLA-PEG$_{600}$-NH$_2$	12	15.5	56.5	62.5
	DHLA-PEG$_{1000}$-NH$_2$	20	21.1	62.1	68.1
Non-reactive ligand	DHLA-PEG$_{750}$-OME	15	17.8	55.8	61.8

[a] The center-to-center separation distance (r) was estimated by combing the QD radius, the PEG size based on the Flory excluded volume calculation and the size of the DHLA group and the ITC linker.

Thus, the only variable parameter in the across the bridge charge transfer interactions between the catechols and the valence band for a given size QDs is the electronic coupling strength (H); H is predicted to exponentially vary with the separation distance (see Fig. 5b):[49–52]

$$H^2 = H^{\circ 2} e^{-\beta r} \quad (7)$$

Here H° is an electronic factor, r is the center-to-center distance, and β is a constant that primarily depends on the nature of the bridge molecule. Examples of β values reported in the literature include β = 1.0–1.4 Å^{-1} for ET in proteins, β = 0.8–1.0 Å^{-1} for ET in saturated hydrocarbon bridges and β = 0.7–1.3 Å^{-1} for ET in polyproline.[50,52] The expression for k_{ET} can be further simplified for a given set of QD–dopamine assemblies where all the parameters are fixed except the electronic coupling H^2 to yield:

$$\ln(k_{ET}) = -\beta r + k_0 \quad (8)$$

where k_0 is a prefactor that depends on the relative alignment of redox levels of the dopamine with respect to the energy levels of the QD (ΔG). Fig. 5c shows a plot of $\ln(k_{ET})$ *vs.* r, using the data shown in Tables 1 and 2 for the conjugates prepared with the yellow- and red-emitting QDs. A linear dependency is observed in both cases, in agreement with the predicted behavior from eqn (8), confirming that the Marcus model for the ET process in these assemblies is valid. We further extracted values for $\beta \cong 0.15$ and 0.13 Å^{-1} for the yellow- and red-emitting ZW/amine-PEG-QD-conjugates, respectively. Conversely, larger k_0 value is extracted for the yellow QD-conjugates ($k_0 \cong 27.5$) than for red QD-conjugates ($k_0 \cong 25.3$). The two main features that emerge from the above analysis are: (1) The values for β are comparable for both sets of QDs, which is anticipated for these assemblies, since the same PEG moieties were used as the bridge molecule. (2) The higher intercept for the yellow-emitting QD-conjugates results from the larger energy mismatch (essentially larger ΔG between the oxidation potential of the catechol and valence band of the QDs).

Conclusion

We have investigated the distance-dependence charge transfer interactions that take place in assemblies of QD–dopamine conjugates coupled *via* a poly(ethylene glycol) (PEG) chain with varying size. The QD PL quenching efficiency as verified by steady-state and time-resolved fluorescence measurements was found to strongly depend on the PEG bridges used, with substantially more pronounced PL losses measured for shorter separation distance and *vice versa*. We were able to successfully correlate the electron transfer rates, k_{ET}, extracted from the fluorescence data, to the Marcus electron transfer model. A clearly-defined exponential dependence of the charge transfer rate on the separation distance was measured for the two sets of QDs. In addition to the effects of separation distance, we found that changing the QD size also affected the measured PL quenching.

We further explored the effects of shielding on the conjugate formation and the ensuing PL losses by comparing data collected using QDs prepared with a compact zwitterion ligands (as the majority inert cap) to those collected from assemblies prepared with a longer inert PEG. We found that PEG coating (larger) shields dopamine access to the reactive amine, resulting in more heterogeneous conjugates and weaker PL quenching. QD–dopamine conjugates prepared with tunable PEG bridges provide promising platforms for constructing biosensors that exploit the unique redox characteristics of dopamine, the size-tunable spectroscopic properties of the QDs and the flexibility afforded by a varying size inert PEG bridge. Such QD–dopamine conjugates assembled *via* a tunable size PEG bridge, a controllable valence, while using a zwitterion-capped QDs are also greatly promising for use in intracellular sensing and imaging. One promising idea worth pursuing is to use the recognition specificity of dopamine to certain metals ions and the cysteine amino acid to assemble specific biological sensors for *in vitro* and/or *in vivo* studies.[53–55]

Acknowledgements

The authors thank FSU, the National Science Foundation (Grant No. 1058957) and Pfizer for financial support.

References

1 C. J. Wang, M. Shim and P. Guyot-Sionnest, Electrochromic nanocrystal quantum dots, *Science*, 2001, **291**, 2390–2392.
2 D. V. Talapin, J. S. Lee, M. V. Kovalenko and E. V. Shevchenko, Prospects of Colloidal Nanocrystals for Electronic and Optoelectronic Applications, *Chem. Rev.*, 2010, **110**, 389–458.

3 A. M. Smith and S. M. Nie, Semiconductor Nanocrystals: Structure, Properties, and Band Gap Engineering, *Acc. Chem. Res.*, 2010, **43**, 190–200.
4 V. I. Klimov, *Nanocrystal quantum dots*, CRC Press, Boca Raton, 2nd edn, 2010, p. xv, p. 469.
5 A. P. Alivisatos, Semiconductor clusters, nanocrystals, and quantum dots, *Science*, 1996, **271**, 933–937.
6 C. B. Murray, C. R. Kagan and M. G. Bawendi, Synthesis and characterization of monodisperse nanocrystals and close-packed nanocrystal assemblies, *Annu. Rev. Mater. Sci.*, 2000, **30**, 545–610.
7 X. G. Peng, L. Manna, W. D. Yang, J. Wickham, E. Scher, A. Kadavanich and A. P. Alivisatos, Shape control of CdSe nanocrystals, *Nature*, 2000, **404**, 59–61.
8 I. Yildiz, E. Deniz and F. M. Raymo, Fluorescence modulation with photochromic switches in nanostructured constructs, *Chem. Soc. Rev.*, 2009, **38**, 1859–1867.
9 M. Amelia, S. Impellizzeri, S. Monaco, I. Yildiz, S. Silvi, F. M. Raymo and A. Credi, Structural and size effects on the spectroscopic and redox properties of CdSe nanocrystals in solution: the role of defect states, *ChemPhysChem*, 2011, **12**, 2280–2288.
10 I. L. Medintz, A. R. Clapp, H. Mattoussi, E. R. Goldman, B. Fisher and J. M. Mauro, Self-assembled nanoscale biosensors based on quantum dot FRET donors, *Nat. Mater.*, 2003, **2**, 630–638.
11 M. Sykora, M. A. Petruska, J. Alstrum-Acevedo, I. Bezel, T. J. Meyer and V. I. Klimov, Photoinduced charge transfer between CdSe nanocrystal quantum dots and Ru-polypyridine complexes, *J. Am. Chem. Soc.*, 2006, **128**, 9984–9985.
12 T. Pons, I. L. Medintz, K. E. Sapsford, S. Higashiya, A. F. Grimes, D. S. English and H. Mattoussi, On the quenching of semiconductor quantum dot photoluminescence by proximal gold nanoparticles, *Nano Lett.*, 2007, **7**, 3157–3164.
13 I. L. Medintz, T. Pons, S. A. Trammell, A. F. Grimes, D. S. English, J. B. Blanco-Canosa, P. E. Dawson and H. Mattoussi, Interactions between Redox Complexes and Semiconductor Quantum Dots Coupled *via* a Peptide Bridge, *J. Am. Chem. Soc.*, 2008, **130**, 16745–16756.
14 H. Mattoussi, G. Palui and H. B. Na, Luminescent quantum dots as platforms for probing *in vitro* and *in vivo* biological processes, *Adv. Drug Delivery Rev.*, 2012, **64**, 138–166.
15 M. H. Stewart, A. L. Huston, A. M. Scott, A. L. Efros, J. S. Melinger, K. B. Gemmill, S. A. Trammell, J. B. Blanco-Canosa, P. E. Dawson and I. L. Medintz, Complex Forster Energy Transfer Interactions between Semiconductor Quantum Dots and a Redox-Active Osmium Assembly, *ACS Nano*, 2012, **6**, 5330–5347.
16 P. T. Snee, R. C. Somers, G. Nair, J. P. Zimmer, M. G. Bawendi and D. G. Nocera, A ratiometric CdSe/ZnS nanocrystal pH sensor, *J. Am. Chem. Soc.*, 2006, **128**, 13320–13321.
17 Y. Chen, R. Thakar and P. T. Snee, Imparting nanoparticle function with size-controlled amphiphilic polymers, *J. Am. Chem. Soc.*, 2008, **130**, 3744–3745.
18 I. Robel, M. Kuno and P. V. Kamat, Size-dependent electron injection from excited CdSe quantum dots into TiO_2 nanoparticles, *J. Am. Chem. Soc.*, 2007, **129**, 4136–4137.
19 R. Freeman, T. Finder, L. Bahshi, R. Gill and I. Willner, Functionalized CdSe/ZnS QDs for the Detection of Nitroaromatic or RDX Explosives, *Adv. Mater.*, 2012, **24**, 6416–6421.
20 A. R. Clapp, I. L. Medintz, J. M. Mauro, B. R. Fisher, M. G. Bawendi and H. Mattoussi, Fluorescence resonance energy transfer between quantum dot donors and dye-labeled protein acceptors, *J. Am. Chem. Soc.*, 2004, **126**, 301–310.
21 R. S. Dibbell and D. F. Watson, Distance-Dependent Electron Transfer in Tethered Assemblies of CdS Quantum Dots and TiO_2 Nanoparticles, *J. Phys. Chem. C*, 2009, **113**, 3139–3149.
22 F. Aldeek, X. Ji and H. Mattoussi, Quenching of Quantum Dot Emission by Fluorescent Gold Clusters: What It Does and Does Not Share with the Forster Formalism, *J. Phys. Chem. C*, 2013, **117**, 15429–15437.
23 Y. Q. Li, L. Y. Guan, H. L. Zhang, J. Chen, S. Lin, Z. Y. Ma and Y. D. Zhao, Distance-dependent metal-enhanced quantum dots fluorescence analysis in solution by capillary electrophoresis and its application to DNA detection, *Anal. Chem.*, 2011, **83**, 4103–4109.
24 R. Gill, R. Freeman, J. P. Xu, I. Willner, S. Winograd, I. Shweky and U. Banin, Probing biocatalytic transformations with CdSe-ZnS QDs, *J. Am. Chem. Soc.*, 2006, **128**, 15376–15377.
25 O. Kovtun, I. D. Tomlinson, D. S. Sakrikar, J. C. Chang, R. D. Blakely and S. J. Rosenthal, Visualization of the Cocaine-Sensitive Dopamine Transporter with Ligand-Conjugated Quantum Dots, *ACS Chem. Neurosci.*, 2011, **2**, 370–378.
26 J. Sedo, J. Saiz-Poseu, F. Busque and D. Ruiz-Molina, Catechol-Based Biomimetic Functional Materials, *Adv. Mater.*, 2013, **25**, 653–701.
27 T. L. Vickrey, N. Xiao and B. J. Venton, Kinetics of the dopamine transporter in Drosophila larva, *ACS Chem. Neurosci.*, 2013, **4**(5), 832–837.
28 K. McFarland, T. A. Spalding, D. Hubbard, J. N. Ma, R. Olsson and E. S. Burstein, Low dose bexarotene treatment rescues dopamine neurons and restores behavioral function in models of Parkinson's disease, *ACS Chem. Neurosci.*, 2013, **4**, 1430–1438.
29 Y. Li, Y. Zhou, B. Qi, T. Gong, X. Sun, Y. Fu and Z. Zhang, Brain-Specific Delivery of Dopamine Mediated by N,N-Dimethyl Amino Group for the Treatment of Parkinson's Disease, *Mol. Pharmaceutics*, 2014, **11**(9), 3174–3185.
30 S. J. Clarke, C. A. Hollmann, Z. J. Zhang, D. Suffern, S. E. Bradforth, N. M. Dimitrijevic, W. G. Minarik and J. L. Nadeau, Photophysics of dopamine-modified quantum dots and effects on biological systems, *Nat. Mater.*, 2006, **5**, 409–417.
31 D. R. Cooper, D. Suffern, L. Carlini, S. J. Clarke, R. Parbhoo, S. E. Bradforth and J. L. Nadeau, Photoenhancement of lifetimes in CdSe/ZnS and CdTe quantum dot-dopamine conjugates, *Phys. Chem. Chem. Phys.*, 2009, **11**, 4298–4310.

32 I. L. Medintz, M. H. Stewart, S. A. Trammell, K. Susumu, J. B. Delehanty, B. C. Mei, J. S. Melinger, J. B. Blanco-Canosa, P. E. Dawson and H. Mattoussi, Quantum-dot/dopamine bioconjugates function as redox coupled assemblies for *in vitro* and intracellular pH sensing, *Nat. Mater.*, 2010, **9**, 676–684.

33 X. Ji, G. Palui, T. Avellini, H. B. Na, C. Yi, K. L. Knappenberger and H. Mattoussi, On the pH-Dependent Quenching of Quantum Dot Photoluminescence by Redox Active Dopamine, *J. Am. Chem. Soc.*, 2012, **134**, 6006–6017.

34 X. Ji, N. S. Makarov, W. Wang, G. Palui, I. Robel and H. Mattoussi, Tuning the Redox Coupling between Quantum Dots and Dopamine in Hybrid Nanoscale Assemblies, *J. Phys. Chem. C*, 2015, **119**, 3388–3399.

35 A. M. Dennis and G. Bao, Quantum Dot–Fluorescent Protein Pairs as Novel Fluorescence Resonance Energy Transfer Probes, *Nano Lett.*, 2008, **8**, 1439–1445.

36 K. E. e. a. Sapsford, Kinetics of metal-affinity driven self-assembly between proteins or peptides and CdSe-ZnS quantum dots, *J. Phys. Chem. C*, 2007, **111**, 11528–11538.

37 T. Pons, I. L. Medintz, X. Wang, D. S. English and H. Mattoussi, Solution-phase single quantum dot fluorescence resonance energy transfer, *J. Am. Chem. Soc.*, 2006, **128**, 15324–15331.

38 K. Tvrdy, P. A. Frantsuzov and P. V. Kamat, Photoinduced electron transfer from semiconductor quantum dots to metal oxide nanoparticles, *Proc. Natl. Acad. Sci. U. S. A.*, 2011, **108**, 29–34.

39 H. Zhu, N. Song and T. Lian, Charging of quantum dots by sulfide redox electrolytes reduces electron injection efficiency in quantum dot sensitized solar cells, *J. Am. Chem. Soc.*, 2013, **135**, 11461–11464.

40 E. Laviron, Electrochemical Reactions with Protonations at Equilibrium. 10. The Kinetics of the Para-Benzoquinone Hydroquinone Couple on a Platinum-Electrode, *J. Electroanal. Chem.*, 1984, **164**, 213–227.

41 P. J. Flory, *Principles of polymer chemistry*, Cornell University Press, Ithaca, 1953, p. 672.

42 P. G. Degennes, Conformations of Polymers Attached to an Interface, *Macromolecules*, 1980, **13**, 1069–1075.

43 P. G. Degennes, Polymers at an Interface - a Simplified View, *Adv. Colloid Interface Sci.*, 1987, **27**, 189–209.

44 J. V. Jokerst, T. Lobovkina, R. N. Zare and S. S. Gambhir, Nanoparticle PEGylation for imaging and therapy, *Nanomedicine*, 2011, **6**, 715–728.

45 R. A. Marcus, On the Theory of Oxidation-Reduction Reactions Involving Electron Transfer. I, *J. Chem. Phys.*, 1956, **24**, 966–978.

46 T. Sakata, K. Hashimoto and M. Hiramoto, New aspects of electron transfer on semiconductor surface: dye-sensitization system, *J. Phys. Chem.*, 1990, **94**, 3040–3045.

47 J. Huang, D. Stockwell, Z. Q. Huang, D. L. Mohler and T. Q. Lian, Photoinduced ultrafast electron transfer from CdSe quantum dots to re-bipyridyl complexes, *J. Am. Chem. Soc.*, 2008, **130**, 5632–5633.

48 K. Tvrdy, P. A. Frantsuzov and P. V. Kamat, Photoinduced electron transfer from semiconductor quantum dots to metal oxide nanoparticles, *Proc. Natl. Acad. Sci. U. S. A.*, 2011, **108**, 29–34.

49 F. D. Lewis, T. Wu, Y. Zhang, R. L. Letsinger, S. R. Greenfield and M. R. Wasielewski, Distance-dependent electron transfer in DNA hairpins, *Science*, 1997, **277**, 673–676.

50 W. B. Davis, W. A. Svec, M. A. Ratner and M. R. Wasielewski, Molecular-wire behaviour in p-phenylenevinylene oligomers, *Nature*, 1998, **396**, 60–63.

51 H. L. Tavernier and M. D. Fayer, Distance Dependence of Electron Transfer in DNA: The Role of the Reorganization Energy and Free Energy, *J. Phys. Chem. B*, 2000, **104**, 11541–11550.

52 D. M. Adams, L. Brus, C. E. D. Chidsey, S. Creager, C. Creutz, C. R. Kagan, P. V. Kamat, M. Lieberman, S. Lindsay, R. A. Marcus, R. M. Metzger, M. E. Michel-Beyerle, J. R. Miller, M. D. Newton, D. R. Rolison, O. Sankey, K. S. Schanze, J. Yardley and X. Y. Zhu, Charge transfer on the nanoscale: Current status, *J. Phys. Chem. B*, 2003, **107**, 6668–6697.

53 U. ElAyaan, E. Herlinger, R. F. Jameson and W. Linert, Anaerobic oxidation of dopamine by iron(III), *J. Chem. Soc., Dalton Trans.*, 1997, 2813–2818.

54 M. J. LaVoie, B. L. Ostaszewski, A. Weihofen, M. G. Schlossmacher and D. J. Selkoe, Dopamine covalently modifies and functionally inactivates parkin, *Nat. Med.*, 2005, **11**, 1214–1221.

55 K. G. Qu, J. S. Wang, J. S. Ren and X. G. Qu, Carbon Dots Prepared by Hydrothermal Treatment of Dopamine as an Effective Fluorescent Sensing Platform for the Label-Free Detection of Iron(III) Ions and Dopamine, *Chem. – Eur. J.*, 2013, **19**, 7243–7249.